Performance Evaluation of QT-RR Adaptation Time Lag Estimation in Exercise Stress Testing

Cristina Pérez, Esther Pueyo, Juan Pablo Martínez, Jari Viik, Leif Sörnmo, *Fellow, IEEE*, and Pablo Laguna, *Fellow, IEEE*

***Abstract*— *Background:* Slower adaptation of the QT interval to sudden changes in heart rate has been identified as a risk marker of ventricular arrhythmia. The gradual changes observed in exercise stress testing facilitates the estimation of the QT-RR adaptation time lag. *Methods:* The time lag estimation is based on the delay between the observed QT intervals and the QT intervals derived from the observed RR intervals using a memoryless transformation. Assuming that the two types of QT interval are corrupted with either Gaussian or Laplacian noise, the respective maximum likelihood time lag estimators are derived. Estimation performance is evaluated using an ECG simulator which models change in RR and QT intervals with a known time lag, muscle noise level, respiratory rate, and more. The accuracy of T-wave end delineation and the influence of the learning window positioning for model parameter estimation are also investigated. *Results:* Using simulated datasets, the results show that the proposed approach to estimation can be applied to any changes in heart rate trend as long as the frequency content of the trend is below a certain frequency. Moreover, using a proper position of the learning window for exercise so that data compensation reduces the effect of nonstationarity, a lower mean estimation error results for a wide range of time lags. Using a clinical dataset, the Laplacian-based estimator shows a better discrimination between patients grouped according to the risk of suffering from coronary artery disease. *Conclusions*: Using simulated ECGs, the performance evaluation of the proposed method shows that the estimated time lag agrees well with the true time lag.**

***Index Terms*— QT-RR modeling, QT-RR adaptation time lag, exercise stress testing, simulated ECGs, coronary artery disease.**

I. Introduction

THE design of non-invasive, ECG-based markers for risk prediction of sudden cardiac death (SCD) is highly desirable [1]. The QT interval, reflecting the total duration of ventricular depolarization and repolarization, and the related heart rate correction have been used as markers to identify cardiac abnormalities that may lead to SCD [2] in the general population [3] and in cohorts of patients with chronic heart failure [4] and myocardial infarction [5].

The QT adaptation time lag in response to sudden changes in heart rate is another marker associated with cardiac arrhythmias and SCD [6]. Normal ranges of the time lag have been defined for different groups of patients, showing that a prolonged time lag is associated with a higher risk of cardiac arrhythmia [5], [7]–[9]. To shed light on cell and tissue mechanisms underlying the time lag and its relation to arrhythmic risk, experimental, clinical, and simulation studies have been performed [10]–[12]. More recently, multiple parameter risk prediction of SCD based on machine learning has been investigated, where not only ECG data is used but also demographic, clinical, electrophysiological, imaging, and genetic data [13]. The authors concluded that such an approach to SCD prediction has been under-applied and incorrectly implemented but is ripe for future investigation. The proposal of novel ECG-derived parameters is a natural part of the investigation.

Since sudden changes in heart rate may not always be present in Holter recordings, we recently proposed a model-based method to estimate the QT adaptation time lag from ECGs recorded during exercise stress testing (EST) [14]. Although the changes during such testing tend to be more gradual than sudden, they are always present and therefore serve as a useful basis for time lag estimation. The time lag was estimated as the delay between observed QT intervals and QT intervals derived from the RR intervals. The results showed that a prolongation of the time lag during exercise, and a shortening during recovery, were associated with a higher risk of coronary artery disease (CAD). Moreover, the difference in time lag between exercise and recovery was significantly larger for low-risk patients than for high-risk patients. These clinical results are promising, but they need to be complemented with results quantifying estimation performance in various conditions.

ECG simulation represents a powerful tool not only for methods development and training in machine learning, but just as much for evaluation and comparison of methods

Manuscript submitted on May 6, 2024. The work was supported by projects PID2022-140556OB-I00, and TED2021-130459B-I00 funded by Spanish Ministry of Science and Innovation (MICINN) and FEDER, by Gobierno de Aragón (Reference Group Biomedical Signal Interpretation and Computational Simulation (BSICoS) T39_23R and project LMP94_21), and the Royal Physiographic Society, Lund, Sweden. The computation was performed at the High Performance computing platform of the NANBIOSIS ICTS *(Corresponding author: Cristina Pérez).*

C. Pérez, E. Pueyo, J.P. Martínez, and P. Laguna are with the Biomedical Signal Interpretation & Computational Simulation Group (BSICoS), Aragón Institute of Engineering Research (I3A), Zaragoza University, Zaragoza, and CIBER-BBN, Spain (cperez@unizar.es).

J. Viik is with the Faculty of Medicine and Health Technology, Tampere University, Finland.

L. Sörnmo is with the Department of Biomedical Engineering, Lund University, Sweden.

performance. Since a gold standard to determine the true time lag is lacking, simulation is particularly well-suited to evaluate the performance of time lag estimation in the presence of QT dynamics with known and controllable properties. A recently proposed simulator was designed to model various cardiac conditions, including arrhythmias of atrial and ventricular origin, QT interval changes related to heart rate, and a known QT-RR time lag [15]. Moreover, the simulator offers statistical, time-varying modeling of muscle noise, motion artifacts, and respiration—components of particular significance when simulating ECGs recorded during exercise.

Novelties of the present study include relaxation of the assumptions associated with the QT-RR model originally proposed in [14], making the time lag estimation well-suited for a wider range of situations. The assumption of linear changes in heart rate trends is extended to apply also to low-frequency trends. The relative order of the two modeling blocks, i.e., a memoryless transformation and a linear filter, is shown to be uncritical, thereby further supporting the proposed approach to time lag estimation. The above-mentioned simulator is used to evaluate the performance of T-wave end delineation during EST using different lead space reduction techniques as well as the error between the estimated and the true time lag for several signal-to-noise ratios (SNRs) and different estimator structures.

The paper is organized as follows. Section II describes the QT-RR model, the different steps of time lag estimation, derived for both Gaussian and Laplacian noise models, and the positioning of learning windows. Sections III and IV describe the simulated and the clinical datasets, respectively. Sections V and VI present and discuss the results, respectively, and Sec. VII provides the main conclusions.

II. Methods

A. T-wave end delineation

The performance of T-wave end delineation is critical in QT interval analysis. In recent studies [9], [14], wavelet-based delineation [16] was preceded by lead space reduction to improve performance, defined by either principal component analysis (PCA) [17] or generalized periodic component analysis (GπCA$_P$) exploiting the fact that the T-wave is 1-to-P-beat periodic [9]. Using the most significant, transformed lead, robust delineation performance was reported for Holter recordings.

Here, for the first time, the performance is evaluated for conditions closely resembling those of EST, using a T-wave end reference. The transformation matrices associated with PCA and GπCA$_P$ are computed in a 150-s window positioned at the onset of the exercise stress test; the matrices are then held fixed throughout the test.

Before lead transformation and delineation is performed, the influence of high-frequency noise is attenuated by forward–backward filtering using a sixth-order Butterworth, lowpass filter (cut-off frequency at 50 Hz). Baseline wander is attenuated using cubic spline interpolation [18].

For each ECG contained in a simulated dataset, the performance is quantified by the root mean square error, denoted ϵ_θ, between T-wave end determined from a noisy and a reference beat, denoted θ_k and θ_k^r, respectively, where k denotes beat index. The reference beat is the same as the noisy beat except that the SNR is very high (using the definition in (8), the SNR is set to 40 dB); using a noise-free reference beat runs the risk to have a singular transformation matrix.

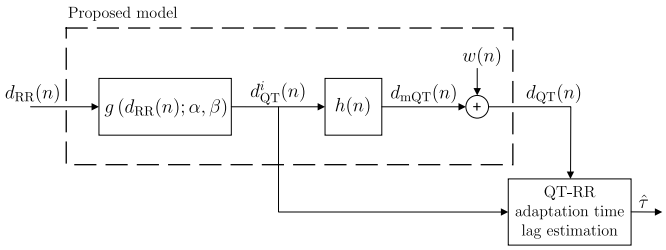

Fig. 1: The proposed model relating the observed RR series $d_{\mathrm{RR}}(n)$ to the observed QT series $d_{\mathrm{QT}}(n)$. The generated output of the memoryless transformation $g\,(d_{\mathrm{RR}}(n);\alpha,\beta)$ is an instantaneous QT series $d^i_{\mathrm{QT}}(n)$ that, when filtered by a linear, time-invariant, first-order filter $h(n)$, models the QT series $d_{\mathrm{mQT}}(n)$. The observed $d_{\mathrm{QT}}(n)$ is modeled as the sum of $d_{\mathrm{mQT}}(n)$ and noise $w(n)$. The QT-RR adaptation time lag τ is estimated as the delay between $d^i_{\mathrm{QT}}(n)$ and $d_{\mathrm{QT}}(n)$.

B. QT-RR modeling

The starting point of QT-RR adaptation time lag estimation is the beat-to-beat observation of RR and QT intervals, resulting in the series $d_{\mathrm{RR}}(k)$ and $d_{\mathrm{QT}}(k)$, respectively. Multilead wavelet-based delineation is used to determine Q-wave onset and R-wave position, whereas the most significant, transformed lead of GπCA$_1$ is used to determine T-wave end as this choice was found to offer better performance, see Sec. V-A. Using interpolation, $d_{\mathrm{RR}}(k)$ and $d_{\mathrm{QT}}(k)$ are then resampled at a rate of 4 Hz, resulting in the uniformly sampled series $d_{\mathrm{RR}}(n)$ and $d_{\mathrm{QT}}(n)$, where n is the sample index.

Time lag estimation builds on the model displayed in Fig. 1, where the delay between $d_{\mathrm{QT}}(n)$ and an instantaneous series $d^i_{\mathrm{QT}}(n)$, related to $d_{\mathrm{RR}}(n)$ through a memoryless transformation, determines the time lag. This transformation, accounting for the QT-RR relation under stationary conditions, is defined by a differentiable function $g(d_{\mathrm{RR}}(n);\alpha,\beta)$ whose shape is determined by the scalar parameters α and β; "stationary" is here to be understood in the broader sense as "non-changing trend". Using the least squares technique, α and β are estimated by fitting $g(d_{\mathrm{RR}}(n);\alpha,\beta)$ either to observed or modified data pairs $[d_{\mathrm{QT}}(n), d_{\mathrm{RR}}(n)]$ contained in three disjoint learning windows with the following positions (window notation is within parenthesis): the first 40 s of rest before exercise (W_b), 20 s either centered around peak exercise or aligned so that the window ends when early recovery begins which depends on the approach taken to window positioning (W_e), cf. Sec II-D), and the last 40 s of recovery (W_{lr}). The window positions are illustrated in Fig. 2(a). Thus, for each patient, α and β are estimated using the data pairs of the concatenated three windows. Together, the concatenated windows $W_b \cup W_e \cup W_{lr}$

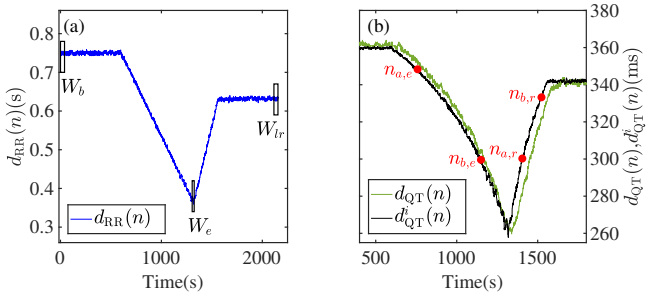

Fig. 2: (a) An observed RR series $d_{\text{RR}}(n)$ and the learning windows positioned at rest (W_b), exercise (W_e), and late recovery, (W_{lr}) indicated by boxes. (b) An observed QT series $d_{\text{QT}}(n)$ and the related instantaneous QT series $d^i_{\text{QT}}(n)$, where the intervals for time lag estimation are delimited by $n_{a,e}$ and $n_{b,e}$ for exercise and $n_{a,r}$ and $n_{b,r}$ for recovery. The series $d_{\text{RR}}(n)$ and $d_{\text{QT}}(n)$ are obtained from a simulated, typical exercise ECG, see Sec. III-A.

should contain a wide range of RR intervals so as to produce a more reliable least squares fit.

At an early stage of the study, the data pairs of these three windows were assumed stationary. However, this assumption was found reasonable only for the resting and recovery windows, but not for the exercise window. Therefore, the data pairs in the exercise window are modified to reduce the effect of nonstationarity, see Sec. II-D.

The output $d^i_{\text{QT}}(n)$ of the memoryless transformation is fed to a linear, time-invariant, first-order filter whose impulse response is given by

$$h(n) = \kappa e^{-n/\tau} u(n), \tag{1}$$

where τ is the memory time constant, expressed in samples, here taken to be the QT-RR adaptation time lag, and $u(n)$ is the unit step function. The output of $h(n)$ is the modeled QT series $d_{\text{mQT}}(n)$, resulting in $d_{\text{QT}}(n)$ once noise $w(n)$ is added accounting for modeling and delineation errors.

In contrast to the original QT-RR model proposed in [19], $g\left(d_{\text{RR}}(n); \alpha, \beta\right)$ is here placed before $h(n)$, not after, see Fig. 1. The two orderings are not mathematically equivalent since $g\left(d_{\text{RR}}(n); \alpha, \beta\right)$ is typically nonlinear. However, if τ is small relative to the time span required for RR intervals to change significantly, it can be shown that the block order is interchangeable, see Appendix I. While it is not clear which order closer models the underlying physiology, the order in Fig. 1 is better suited for estimation of τ as it allows $d^i_{\text{QT}}(n)$ to be paired with $d_{\text{QT}}(n)$.

For simulated ECGs, the accuracy of the parameter estimates $\hat{\alpha}$ and $\hat{\beta}$ is characterized by their respective means $m_{\hat{\alpha}}$, $m_{\hat{\beta}}$ and standard deviations $\sigma_{\hat{\alpha}}$, $\sigma_{\hat{\beta}}$. The estimates are based on the data pairs in the three learning windows.

C. QT-RR adaptation time lag estimation

When the input to a first-order filter $h(n)$ is a linear ramp, it is well-known that the output is a delayed linear ramp [20]. Since $d_{\text{RR}}(n)$ often exhibits such a ramp-like behavior during exercise as well as recovery, $d^i_{\text{QT}}(n)$ will do so as well—a result which is central to time lag estimation. Figure 2(b) presents an example where the delay between $d_{\text{QT}}(n)$ and $d^i_{\text{QT}}(n)$ is clearly discernible, serving as an estimate of τ.

When $d_{\text{RR}}(n)$ is better characterized by a low-frequency trend, denoted $s(n)$, than by a linear ramp, it can be shown that $h(n)$ still behaves as a time-delay system provided that the spectral content of $s(n)$ is below a certain frequency, see Appendix II for derivation. This result is elucidated by the following expression which shows that the discrete-time Fourier transform of $h(n)$ in (1) is approximately that of a time-delay system,

$$H(\omega) = \frac{\kappa}{1 - e^{-1/\tau} e^{-j\omega}} \approx \frac{\kappa e^{1/\tau}}{e^{1/\tau} - 1} e^{-j\omega\tau}. \tag{2}$$

This result motivates the introduction of the following statistical model of $d^i_{\text{QT}}(n)$ and $d_{\text{QT}}(n)$:

$$\begin{aligned} d^i_{\text{QT}}(n) &= s(n) + v^i(n), \\ d_{\text{QT}}(n) &= s(n-\tau) + v(n), \end{aligned} \qquad n = 0, ..., N-1, \tag{3}$$

where both $v^i(n)$ and $v(n)$ account for short-term, beat-to-beat QT variability and delineation errors. The noise components $v^i(n)$ and $v(n)$ are assumed white, modeled by Laplacian or Gaussian distributions, and statistically independent as $v(n)$ reflects uncertainty in Q-wave onset and T-wave end whereas $v^i(n)$ reflects uncertainty in R-wave position. The statistical parameters, i.e., location and scale of the probability density functions, are assumed identical for $v^i(n)$ and $v(n)$. The integer N is the length of the interval, containing either the exercise or the recovery trend.

Using the maximum likelihood technique, the two estimators of τ can be defined by the same equation but with different exponents of the integrand [21]:

$$\hat{\tau}_p = \arg \min_{-I \le \tau \le I} \sum_{n=n_a}^{n_b} |d^i_{\text{QT}}(n) - d_{\text{QT}}(n+\tau)|^p, \quad p = 1, 2, \tag{4}$$

where $\hat{\tau}_1$ and $\hat{\tau}_2$ relate to Laplacian and Gaussian noise, respectively, and the delay τ is contained in the search range $[-I, I]$. Thus, the maximum likelihood estimators are identical to minimizing either the least absolute error ($p = 1$, Laplacian) or the least squares error ($p = 2$, Gaussian) between $d^i_{\text{QT}}(n)$ and $d_{\text{QT}}(n + \tau)$. It should be noted that neither $s(n)$ nor the statistical parameters need to be known to compute $\hat{\tau}_p$.

The minimization interval $[n_a, n_b]$ is determined using the algorithm in [14]. Since $\hat{\tau}_p$ is estimated both during exercise (e) and recovery (r), yielding $\hat{\tau}_{p,e}$ and $\hat{\tau}_{p,r}$, respectively, two minimization intervals are determined from $d^i_{\text{QT}}(n)$ as described next. The exercise onset $n_{a,e}$ is defined in the time series $d^i_{\text{QT}}(n)$ as the intercept between the flat interval during rest and the linearly decreasing trend during exercise computed from $d_{\text{RR}}(n)$. The same idea is employed to define the recovery end $n_{b,r}$, using the early and late part of recovery. Exercise end $n_{b,e}$, and thus recovery onset $n_{a,r}$, are established at 55% of the total span of their respective areas in $d^i_{\text{QT}}(n)$, away from peak exercise. The onset and end of the intervals used for time lag estimation during exercise and recovery are exemplified in Fig. 2(b).

Using simulated ECGs, estimation performance is quantified by the error ϵ_τ between the estimated time lag $\hat{\tau}_{p,x}$ and the true time lag $\tau_{p,x}$,

$$\epsilon_\tau(p,x) = \hat{\tau}_{p,x} - \tau_{p,x}, \quad p = 1,2; \ x \in \{e,r\}. \tag{5}$$

Thus, in total, four estimates $\hat{\tau}_{p,x}$ are computed for each simulated ECG.

The difference between $\hat{\tau}_{p,e}$ and $\hat{\tau}_{p,r}$ is also computed, being of particular interest using clinical ECGs.

$$\Delta\hat{\tau}_p = \hat{\tau}_{p,r} - \hat{\tau}_{p,e}, \quad p = 1,2. \tag{6}$$

D. Data-dependent modification of the learning window data pairs at peak exercise

Estimation of the model parameters α and β is based on the assumption that $[d_{\text{QT}}(n), d_{\text{RR}}(n)]$ are observed under stationary conditions in the three learning windows at fixed positions, cf. Section II-B. Since this assumption rarely holds for the data pairs in the window centered at peak exercise, this problem can to some extent be reduced by replacing $[d_{\text{QT}}(n), d_{\text{RR}}(n)]$ with $[d_{\text{QT}}(n) - \Delta_{\text{QT}}, d_{\text{RR}}(n)]$. The decrement Δ_{QT} accounts for the additional shortening of $d_{\text{QT}}(n)$, corresponding to $d_{\text{QT}}(n)$ that would have been obtained provided that $d_{\text{RR}}(n)$ had remained stationary long enough at peak exercise until $[d_{\text{QT}}(n), d_{\text{RR}}(n)]$ would have become stationary. The computation of Δ_{QT} is data-dependent as it involves both $d_{\text{QT}}(n)$ and $d^i_{\text{QT}}(n)$, see [14] for details. Since the use of $[d_{\text{QT}}(n) - \Delta_{\text{QT}}, d_{\text{RR}}(n)]$ yields other estimates of α and β, the modified instantaneous QT series is denoted $\tilde{d}^i_{\text{QT}}(n)$.

To deal even better with the above assumption, the end of the exercise window is, in addition to modifying $d_{\text{QT}}(n)$ with Δ_{QT}, aligned to the time for peak exercise, denoted $\check{W}_e$, so that only data pairs from exercise are used. For the modified and aligned window, the resulting instantaneous QT series is denoted $\check{d}^i_{\text{QT}}(n)$.

Thus, the following three definitions of the instantaneous QT series are studied: $d^i_{\text{QT}}(n)$, $\tilde{d}^i_{\text{QT}}(n)$, and $\check{d}^i_{\text{QT}}(n)$. The block diagram in Fig. 3 shows the procedure to estimate α and β using data pairs in the three concatenated windows $W_b \cup \left(W_e \text{ or } \check{W}_e\right) \cup W_{lr}$.

III. Simulated Datasets

To evaluate estimation performance, the recently published, open access ECG simulator is adopted, offering a rich variety of features [15]. The following features are of particular significance for the present study: a) user-defined heart rate trends, b) inclusion of muscle noise and motion artifacts with time-varying properties, commonly observed during exercise and recovery, and c) full control of τ.

The simulations rely mostly on the default settings given in [15], including the hyperbolic, memoryless transformation,

$$g(d_{\text{RR}}(n); \alpha, \beta) = \beta + \frac{\alpha}{d_{\text{RR}}(n)}. \tag{7}$$

However, the modeling of RR intervals, muscle noise, motion artifacts, and respiratory rate are modified to account for pertinent characteristics of the four phases that together form an EST, i.e., rest (for notational reasons referred to as basal),

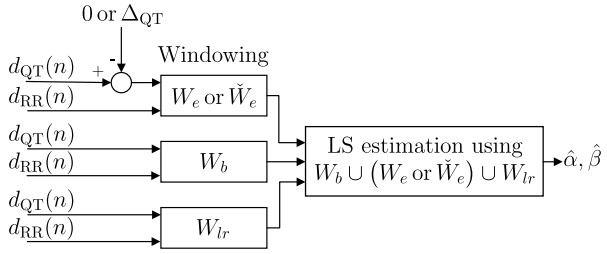

Fig. 3: Estimation of α and β, defining the memoryless transformation $g(d_{\text{RR}}(n); \alpha, \beta)$, is based on $[d_{\text{QT}}(n), d_{\text{RR}}(n)]$ in the three concatenated learning windows. Using an unmodified $d_{\text{QT}}(n)$ windowed with W_e the instantaneous QT series becomes $d^i_{\text{QT}}(n)$. Using $d_{\text{QT}}(n)$ windowed with W_e but modified with Δ_{QT} the instantaneous QT series becomes $\tilde{d}^i_{\text{QT}}(n)$. Using $d_{\text{QT}}(n)$ modified with Δ_{QT} and windowed with $\check{W}_e$ the instantaneous QT series becomes $\check{d}^i_{\text{QT}}(n)$. LS, least square.

exercise, early recovery, and late recovery, whose respective endpoints are denoted t_b, t_e, t_{er}, and t_{lr}. The statistics of the duration of exercise and early recovery were determined from 25 tests [22], whereas the first and the last phase were set to 10 min.

Three different datasets are generated, each of them consisting of 400 simulated, standard 12-lead ECGs, sampled at a rate of 1000 Hz.

A. Simulated, typical exercise ECGs

This dataset, named $\mathcal{D}_t$, contains simulated ECGs defined by a template RR interval pattern mimicking typical EST trends. This template is defined by four phases: 1) constant mean RR interval during rest, $[0, t_b]$, 2) linearly decreasing trend of RR interval during exercise, $[t_b, t_e]$, 3) linearly increasing trend of RR interval during early recovery, $[t_e, t_{er}]$, and 4) constant mean RR interval during late recovery, $[t_{er}, t_{lr}]$. The defining values of phase 1, phase 4, and end of phase 2 of the RR template were obtained by computing the inter-patient mean of intra-patient RR interval means at rest, recovery and exercise learning windows, respectively, using ECGs from 213 patient with low risk of CAD [14]. The series $d_{\text{RR}}(n)$ is obtained by adding variability to the RR interval template trend, using the model in [23]. Figure 4(a) illustrates a template RR interval trend and a simulated pattern $d_{\text{RR}}(n)$ across the four phases.

A template pattern is also provided for the variance of the muscle noise, defined by the four phases: 1) constant, 2) linearly increasing to become four times higher at t_e than at t_b, 3) linearly decreasing until t_{er}, and 4) identical to the constant in phase 1. Together with the generated muscle noise, motion artifacts are randomly included with an occurrence probability of 40%, see [15] for details.

The SNR at peak exercise is defined by

$$\text{SNR} = 20\log_{10}\left(\frac{A_{\text{QRS}}}{\text{RMS}_{\text{noise}}}\right), \tag{8}$$

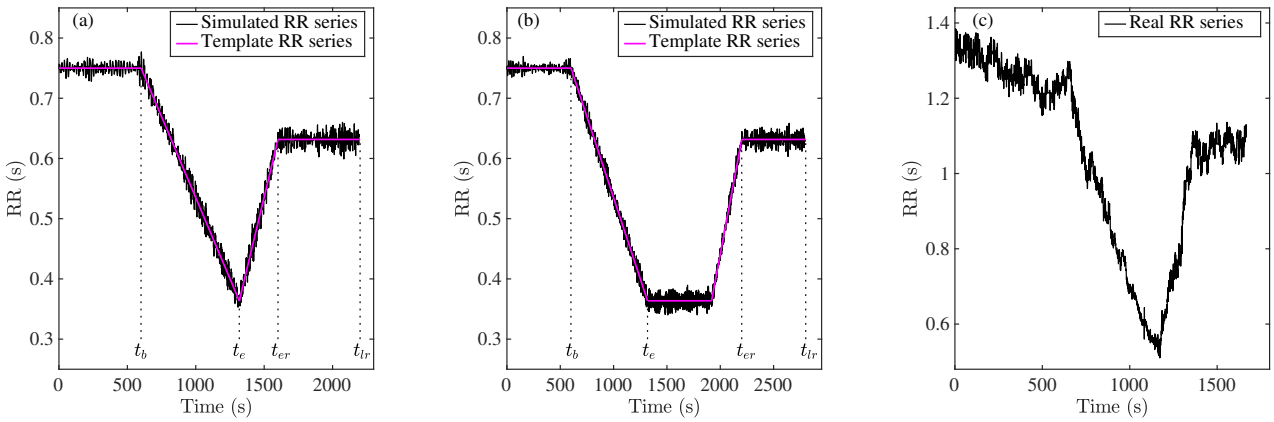

Fig. 4: Template RR interval pattern and observed RR interval series $d_{\mathrm{RR}}(n)$ extracted from the datasets (a) $\mathcal{D}_t$, containing typical exercise ECGs with the four phases (rest ending at t_b, exercise at t_e, early recovery at t_{er}, and late recovery at t_{lr}), (b) $\mathcal{D}_{ee}$, containing exercise ECGs with extended exercise, and (c) $\mathcal{D}_r$, containing exercise ECGs using real RR intervals.

where A_{QRS} is the peak-to-peak amplitude of the ensemble-averaged QRS complex, determined in a 100-ms interval centered around the R-peak, see [9], [24] for details. The muscle noise signal is rescaled so that its RMS value in a window of 60 s at peak exercise equals $\mathrm{RMS}_{\mathrm{noise}}$. All leads are assumed to have the same SNR. Simulated ECGs at different SNRs are exemplified in Fig. 5.

The respiratory rate changes across the four phases according to a template pattern similar to the one defined for the muscle noise variance [24]: 1) constant, 2) linearly increasing until t_e, 3) linearly decreasing until t_{er}, and 4) identical to the constant in phase 1. This respiratory rate modulates heart rate variability and QRS-T complex morphology [15].

The dataset $\mathcal{D}_t$ is obtained by simulating 25 ECGs for all combinations of τ and SNR, assuming the following values:

$$\tau = \{20, 30, 40, 50\} \text{ s}, \tag{9}$$

$$\mathrm{SNR} = \{27, 30, 35, 40\} \text{ dB}, \tag{10}$$

where the different SNRs correspond the following RMS values: $\{45, 32, 18, 10\}$ μV. Thus, in total, $\mathcal{D}_t$ contains $25 \cdot 4 \cdot 4 = 400$ ECGs.

B. Simulated exercise ECGs with extended peak exercise

This dataset, named $\mathcal{D}_{ee}$, is generated in exactly the same way as $\mathcal{D}_t$, except that peak exercise is extended for 10 min with constant mean RR interval, constant muscle noise variance, and constant respiratory rate, see Fig. 4(b). When analyzing $\mathcal{D}_{ee}$, the end of the exercise learning window is aligned to the onset of early recovery. This positioning ensures that both the observed QT interval and the observed heart rate at peak exercise have become stationary, and, accordingly, α and β can be estimated from stationary data in the three learning windows.

Moreover, $\mathcal{D}_{ee}$ makes it possible to study the effect of nonstationarity in the exercise window separately from the effect of selecting data pairs from just three windows during EST.

TABLE I: User-defined simulation parameters.

	Phase	$\mathcal{D}_t$	$\mathcal{D}_{ee}$	$\mathcal{D}_r$
Mean duration of the exercise stress tests (min)	rest	10	10	5
	exercise	12	12	8
	extended peak exercise	–	10	–
	early recovery	5	5	3
	late recovery	10	10	4
Mean heart rate (beats per min)	rest	80	80	69
	peak exercise	165	165	139
	end of early recovery	95	95	81
Respiratory rate (breaths per min)	rest	15	15	–
	peak exercise	42	42	–
	end of early recovery	18	18	–

C. Simulated exercise ECGs using real RR intervals

This dataset, named $\mathcal{D}_r$, is generated using 25 different RR series from exercise stress tests [25], one of them displayed in Fig. 4(c). The use of real RR series as input to the simulator is motivated by the observation that RR trends during exercise and recovery can deviate considerably from a linear ramp, which makes the use of real RR series a valuable complement to simulated RR series when evaluating the performance of time lag estimation. While the evaluation could have been based on simulated linear ramps exclusively, the use of real RR series is a means to validate the derivation in Appendix II, showing that the estimation of τ is equally valid as long as the deviation of the trends from a linear ramp is sufficiently low-frequency.

The parameters defining the mean duration of exercise stress tests, heart rate, and respiratory rate of the three simulated datasets are listed in Table I.

IV. Clinical Dataset

To further evaluate the performance of the time lag estimators in (4), a clinical dataset was analyzed, consisting of 448 ECGs recorded from patients undergoing EST at Tampere University Hospital in Finland [25]. The patients are classified into

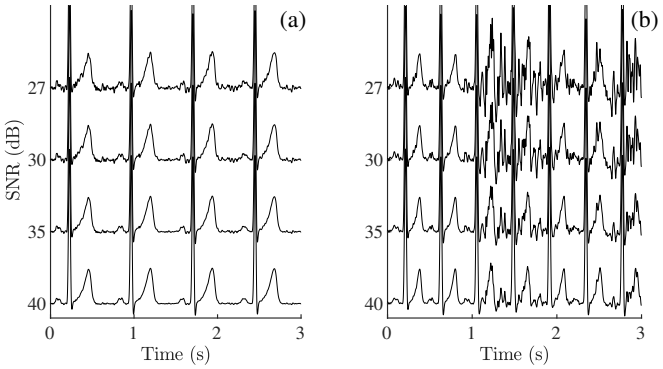

Fig. 5: Simulated ECGs (lead V_4) with different SNRs at (a) low or (b) high heart rate.

TABLE II: Mean and standard deviation of the T-wave end delineation error ϵ_θ, $m_{\epsilon_\theta} \pm \sigma_{\epsilon_\theta}$ (ms) for different types of lead space reduction and SNRs. The results are based on $\mathcal{D}_t \cup \mathcal{D}_r$ and includes all values of τ listed in (9), yielding a total of 600 ECGs.

SNR	27 dB	30 dB	35 dB
GπCA$_1$	3.2* $\pm$ 1.8	2.1 $\pm$ 1.1	1.0 $\pm$ 0.5
GπCA$_3$	3.3* $\pm$ 1.8	2.2 $\pm$ 1.1	1.1 $\pm$ 0.6
PCA	3.7 $\pm$ 2.4	2.3 $\pm$ 1.5	0.9 $\pm$ 0.6

*p-value of a t-test when comparing GπCA$_1$ vs PCA ($p = 0.01$), and GπCA$_3$ vs PCA ($p = 0.05$) for an SNR of 27 dB.

four groups according to their likelihood of suffering CAD. The low-risk ECG group (ECG-LR) was identified based on clinical history and ECG interpretation. The remaining patients underwent coronary angiography (COR) to determine the percentage of luminal diameter narrowing in at least one major epicardial coronary artery or main branches, resulting in groups with low risk (COR-LR), middle risk (COR-MR), and high risk (COR-HR). These three groups include patients with an occlusion of less than 50%, between 50 and 75%, and 75% or more, respectively. The ECG-LR, COR-LR, COR-MR, and COR-HR groups have 213, 59, 24, and 152 patients, respectively.

V. Results

A. T-wave end delineation

For the union of $\mathcal{D}_t$ and $\mathcal{D}_r$, the mean bias m_{ϵ_θ} and the standard deviation σ_{ϵ_θ} of the delineation error ϵ_θ is presented in Table II for different types of lead space reduction and SNRs. The results show that both GπCA$_1$ and GπCA$_3$ offer better performance than PCA at the lowest SNR with statistical significance (p-values of 0.01 and 0.05, respectively), whereas the difference in m_{ϵ_θ} becomes smaller at higher SNRs. The lowest m_{ϵ_θ} is obtained for GπCA$_1$, and, therefore, this technique was selected to compute the T-wave end needed in Sec. II-B. It should be noted that the statistical significance reported in Table II depends on the number of simulations, and, consequently, only comparisons in relative terms are meaningful.

TABLE III: Mean $m_{\hat{\alpha}}$ and standard deviation $\sigma_{\hat{\alpha}}$ computed for different datasets and definitions of the instantaneous QT series.

Simulated value		α		β	
		-0.090		0.490	
Estimates obtained from dense sampling of $g(d_{\text{RR}}(n);\alpha,\beta)$		$\hat{\alpha}_s$		$\hat{\beta}_s$	
		-0.078		0.461	
Dataset	Instant. QT series	$m_{\hat{\alpha}}$	$\sigma_{\hat{\alpha}}$	$m_{\hat{\beta}}$	$\sigma_{\hat{\beta}}$
$\mathcal{D}_{ee}$	$d^i_{\text{QT}}(n)$	-0.078	0.005	0.459	0.012
$\mathcal{D}_t$	$d^i_{\text{QT}}(n)$	-0.074	0.004	0.454	0.011
	$\tilde{d}^i_{\text{QT}}(n)$	-0.078	0.004	0.460	0.010
	$\check{d}^i_{\text{QT}}(n)$	-0.078	0.004	0.460	0.010
$\mathcal{D}_r$	$d^i_{\text{QT}}(n)$	-0.074	0.005	0.456	0.012
	$\tilde{d}^i_{\text{QT}}(n)$	-0.079	0.005	0.460	0.012
	$\check{d}^i_{\text{QT}}(n)$	-0.079	0.005	0.460	0.012

B. Estimation of α and β

Table III presents the mean $m_{\hat{\alpha}}$ and the standard deviation $\sigma_{\hat{\alpha}}$ of $\hat{\alpha}$ and $\hat{\beta}$ for the three definitions of the instantaneous QT series, i.e., $d^i_{\text{QT}}(n)$, $\tilde{d}^i_{\text{QT}}(n)$, and $\check{d}^i_{\text{QT}}(n)$; α and β have been assigned values identical to those used for simulation in [15]. The main observation to be made from Table III is that $\hat{\alpha}$ and $\hat{\beta}$ are both biased since $m_{\hat{\alpha}}$ and $m_{\hat{\beta}}$ deviate considerably from their respective true values. This observation applies to $\mathcal{D}_t$, $\mathcal{D}_r$ as well as $\mathcal{D}_{ee}$.

The origin of the bias can be understood by an experiment in which $\hat{\alpha}$ and $\hat{\beta}$ are studied using a simulated ECG whose template RR series decreases stepwise from exercise onset to end, here taken to be 10 steps, each with a 5-min duration. The last part of each step is then used as a learning window with stationary conditions, thereby providing denser sampling of data pairs when fitting $g(d_{\text{RR}}(n);\alpha,\beta)$ than that provided by the typical template RR pattern from EST. The estimates of α and β resulting from using the data pairs of each step, denoted $\hat{\alpha}_s$ and $\hat{\beta}_s$, are much closer to those obtained from $\mathcal{D}_t$, $\mathcal{D}_r$, as well as $\mathcal{D}_{ee}$, see Table III.

C. QT-RR adaptation time lag estimation using $\mathcal{D}_t$ and $\mathcal{D}_r$

Estimation performance is investigated for the time lags and SNRs given in (9) and (10), respectively. The results are expressed in terms of mean bias m_{ϵ_τ} and standard deviation σ_{ϵ_τ} of the time lag error ϵ_τ, cf. (5), and presented for exercise and recovery separately. Using $d^i_{\text{QT}}(n)$, $\tilde{d}^i_{\text{QT}}(n)$, and $\check{d}^i_{\text{QT}}(n)$ in combination with the Laplacian noise assumption, the results obtained from $\mathcal{D}_t$ and $\mathcal{D}_r$ are presented in Fig. 6. The reason for presenting results based on the Laplacian noise assumption on, but not the Gaussian, is provided at the end of this subsection.

Using $d^i_{\text{QT}}(n)$, $\tau_{1,e}$ is typically underestimated during exercise since m_{ϵ_τ} is negative, while $\tau_{1,r}$ is typically overestimated during recovery since m_{ϵ_τ} is positive. Moreover, m_{ϵ_τ} increases as τ becomes increasingly longer. This tendency can be observed by analyzing the difference between the time lag estimates obtained during recovery and exercise, i.e., $\Delta\hat{\tau}_p$: the

This article has been accepted for publication in IEEE Transactions on Biomedical Engineering. This is the author's version which has not been fully edited and content may change prior to final publication. Citation information: DOI 10.1109/TBME.2024.3410008

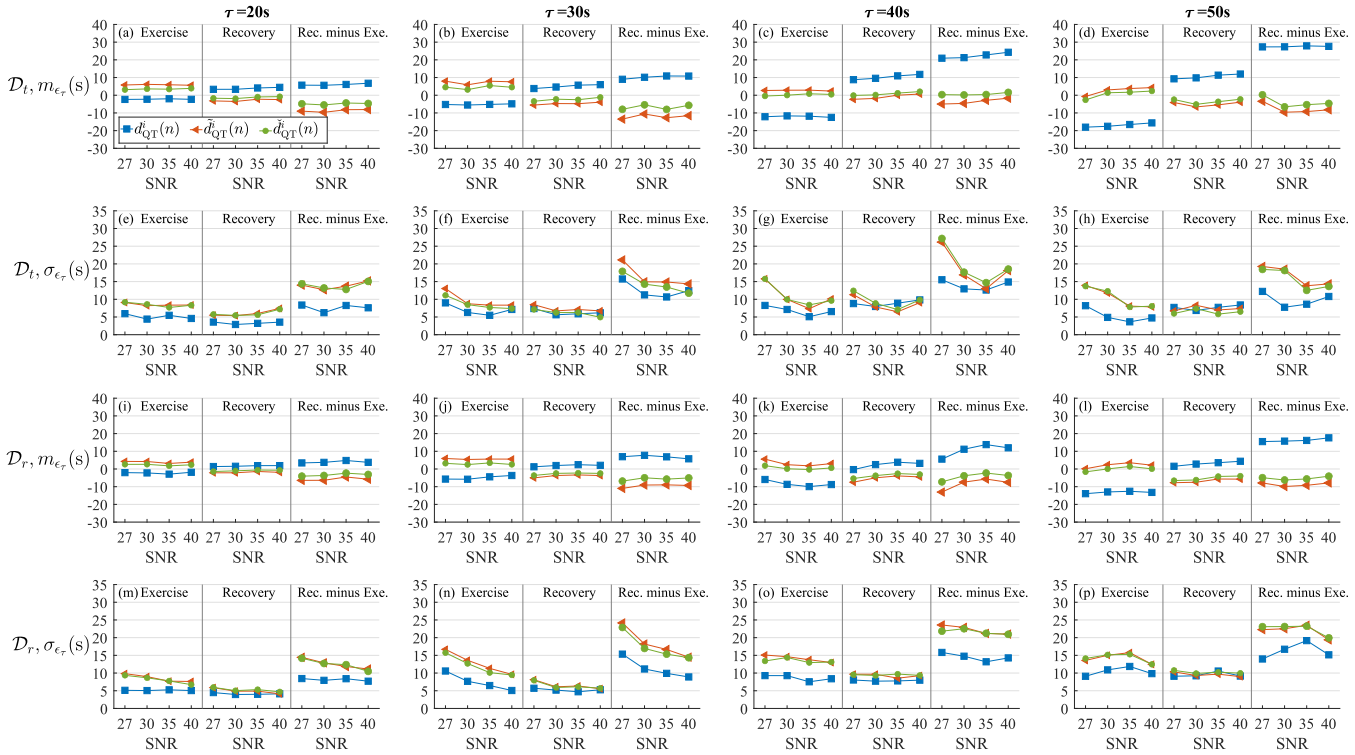

Fig. 6: Mean m_{ϵ_τ} and standard deviation σ_{ϵ_τ} of the time lag error ϵ_τ in exercise, recovery, and the difference between the two time lag estimates, computed for different values of τ (columns), SNRs (horizontal axis), and definitions of the instantaneous QT series. The results for $\mathcal{D}_t$ are shown in (a)–(d) and (e)–(h), respectively. Panels (i)–(l) and (m)–(p) show m_{ϵ_τ} and σ_{ϵ_τ} for $\mathcal{D}_r$. Errors computed with $d^i_{\mathrm{QT}}(n)$, $\tilde{d}^i_{\mathrm{QT}}(n)$, and $\check{d}^i_{\mathrm{QT}}(n)$ are represented by blue, orange, and green colors, respectively. The results are based on the Laplacian noise assumption.

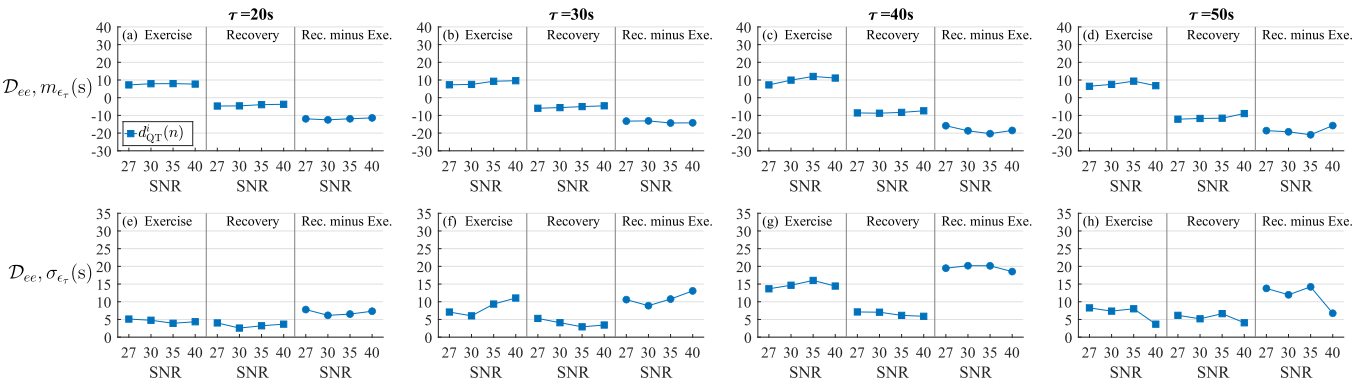

Fig. 7: Mean m_{ϵ_τ} and standard deviation σ_{ϵ_τ} of the time lag error ϵ_τ for $\mathcal{D}_{ee}$ in exercise, recovery, and the difference between the two time lag estimates, computed for different values of τ (columns) and SNRs (horizontal axis) are shown in (a)–(d) and (e)–(h), respectively. The results are based on $d^i_{\mathrm{QT}}(n)$ and the Laplacian noise assumption.

larger the time lag, the larger the bias. Since the time lag in the simulated ECGs is the same during exercise and recovery, a value of $\Delta\hat{\tau}_p$ closer to 0 indicates that the method offers more accurate estimation. These observations apply to both $\mathcal{D}_t$ and $\mathcal{D}_r$, see Figs. 6(a)–(d) and (i)–(l), respectively.

Using $\tilde{d}^i_{\mathrm{QT}}(n)$ and $\check{d}^i_{\mathrm{QT}}(n)$, the under- and overestimation become less pronounced than for $d^i_{\mathrm{QT}}(n)$, where $\check{d}^i_{\mathrm{QT}}(n)$ is the better choice of the two. In addition, m_{ϵ_τ} is essentially independent of τ for $\tilde{d}^i_{\mathrm{QT}}(n)$ and $\check{d}^i_{\mathrm{QT}}(n)$. The estimate $\Delta\hat{\tau}_p$ is closer to 0 for $\check{d}^i_{\mathrm{QT}}(n)$ than for $\tilde{d}^i_{\mathrm{QT}}(n)$, confirming a more accurate estimation when using the modified and aligned learning window at exercise $\check{W}_{\mathrm{e}}$. However, the improvement in m_{ϵ_τ} for $\tilde{d}^i_{\mathrm{QT}}(n)$ and $\check{d}^i_{\mathrm{QT}}(n)$ is traded for a larger σ_{ϵ_τ} during exercise, whereas σ_{ϵ_τ} differs only slightly between $d^i_{\mathrm{QT}}(n)$, $\tilde{d}^i_{\mathrm{QT}}(n)$, and $\check{d}^i_{\mathrm{QT}}(n)$ during recovery. Again, these observations apply to both $\mathcal{D}_t$ and $\mathcal{D}_r$, see Figs. 6(e)–(h) and (m)–(p), respectively.

In general, m_{ϵ_τ} is not much influenced by the SNR when analyzing $\mathcal{D}_t$ and $\mathcal{D}_r$, whereas σ_{ϵ_τ} decreases for an increasing SNR.

The results obtained from $\mathcal{D}_t$ and $\mathcal{D}_r$ are quite similar, thus supporting the derivation in Appendix II which shows that $s(n)$ does not have to be a linear ramp but it can indeed be a trend whose spectral content is below a certain frequency.

To study the statistical distribution of the QT intervals, the histogram of the difference $d_{QT}(k) - \bar{d}_{QT}(k)$ was computed, where $d_{QT}(k)$ is the QT interval of the k-th beat and $\bar{d}_{QT}(k)$ is the running median QT interval of five consecutive beats. Then, in the least square error sense, the best fit of the Laplacian and the Gaussian probability density functions to the histogram was determined. Using the simulated/real datasets, the errors associated with the Laplacian assumption were 0.0076/0.0029, whereas the errors associated with the Gaussian assumption were 0.0099/0.0045, thus justifying the use of the Laplacian assumption. Since, on the simulated datasets, the Gaussian assumption leads to results which are very similar to those of the Laplacian assumption, they are not presented.

D. QT-RR adaptation time lag estimation using $\mathcal{D}_{ee}$

Peak exercise in $\mathcal{D}_{ee}$ is extended by 10 min to ensure that the exercise window is stationary. Therefore, only $d^i_{QT}(n)$ is relevant to use when analyzing this dataset, while $\tilde{d}^i_{QT}(n)$ and $\check{d}^i_{QT}(n)$ are not as they aim to reduce the nonstationarity of the exercise window. By comparing the results obtained from $\mathcal{D}_{ee}$ with those from $\mathcal{D}_t$ and $\mathcal{D}_r$, the extent with which the estimation of τ is influenced by nonstationarity is indicated.

The results from $\mathcal{D}_{ee}$ show that $\tau_{1,e}$ and $\tau_{1,r}$ are over- and underestimated, respectively, see Figs. 7(a)–(d), which stand in contrast to the results obtained from $\mathcal{D}_t$ and $\mathcal{D}_r$ where $\tau_{1,e}$ and $\tau_{1,r}$ are under- and overestimated, respectively, cf. Sec V-C. This difference in time lag bias is unexpected since the data in the exercise window is stationary. This result is likely explained by the reduced RR interval range in this window when compared to the exercise window of $\mathcal{D}_t$ or $\mathcal{D}_r$.

The importance of the RR interval range is illustrated in Fig. 8 where $[d_{QT}(n), d_{RR}(n)]$ are displayed for the three learning windows together with fitted functions $g(d_{RR}(n); \hat{\alpha}, \hat{\beta})$. Using $d^i_{QT}(n)$ on $\mathcal{D}_t$ and $\mathcal{D}_{ee}$, the better fit is obtained from $\mathcal{D}_{ee}$. However, the best fit is obtained when using $\check{d}^i_{QT}(n)$ on $\mathcal{D}_t$. These observations corroborate the results in Sec. V-C supporting the selection of $\check{d}^i_{QT}(n)$. The performance achieved with $\check{d}^i_{QT}(n)$ is explained by better handling of the nonstationarity in the exercise window and the wider RR interval range of the three learning windows.

E. Clinical evaluation in CAD patients

Using the clinical dataset, the discriminatory power to classify different levels of cardiac risk in CAD patients is evaluated for $\hat{\tau}_{p,e}$, $\hat{\tau}_{p,r}$, and $\Delta\hat{\tau}_p$. These estimates are obtained using the hyperbolic transformation and $\check{d}^i_{QT}(n)$, where the latter choice is motivated by the better performance obtained on simulated ECGs, see Secs. V-C and V-D.

Figures 9(a)–(b) present the comparative results when $\hat{\tau}_{p,e}$ and $\hat{\tau}_{p,r}$ are used for evaluation of the four risk groups. During exercise, the ECG-LR/COR-HR and COR-LR/COR-HR groups can be discriminated with statistical significance

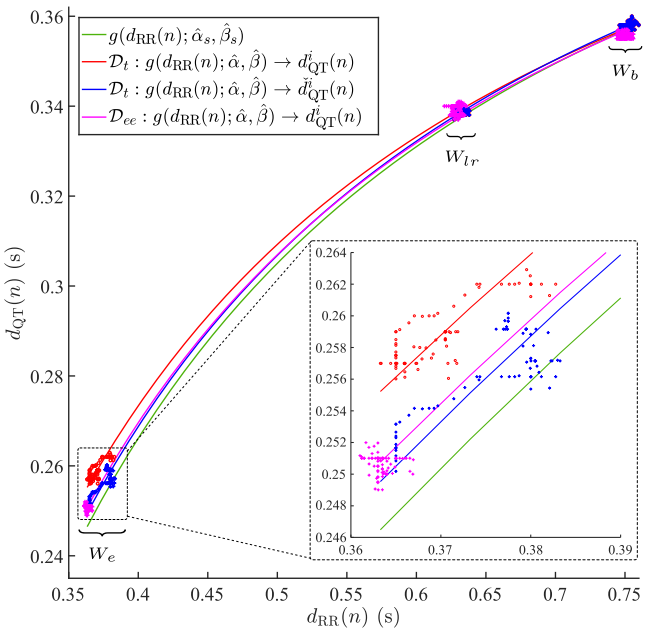

Fig. 8: The two data pairs $[d_{QT}(n), d_{RR}(n)]$ and $[d_{QT}(n) - \Delta_{QT}, d_{RR}(n)]$ of the three learning windows, the memoryless transformation $g(d_{RR}(n); \hat{\alpha}, \hat{\beta})$ with estimated parameters, and the reference $g(d_{RR}(n); \hat{\alpha}_s, \hat{\beta}_s)$ described in Sec. V-B. The three clusters of data pairs originate from the exercise W_e, the recovery W_{lr}, and the resting W_b windows (left to right). The examples are taken from $\mathcal{D}_t$ and $\mathcal{D}_{ee}$. For reasons of clarity, the results for $\tilde{d}^i_{QT}(n)$ are omitted.

for both the Laplacian and the Gaussian-based estimators; during recovery, this significance extends to also include ECG-LR/COR-MR. No significant difference is found for the results obtained using the two types of estimators.

Figure 9(c) shows that the Laplacian-based estimator offers greater discriminatory power of $\Delta\hat{\tau}_p$, $p = 1, 2$. This result, together with the better fit of a Laplacian probability density function to the QT histogram, shows that the Laplacian assumption is advantageous.

VI. Discussion

A. QT-RR adaptation time lag estimation

The main aim of the present study is to evaluate whether the time delay between $d_{QT}(n)$ and an instantaneous QT series, either given by $d^i_{QT}(n)$, $\tilde{d}^i_{QT}(n)$, or $\check{d}^i_{QT}(n)$, can serve as a surrogate for estimating the QT-RR adaptation time lag. The results show that the data-dependent modification of the data pairs in the exercise window yields better performance than the unmodified data pairs, i.e., $\tilde{d}^i_{QT}(n)$ and $\check{d}^i_{QT}(n)$ yield better performance than $d^i_{QT}(n)$. While the mean bias m_{ϵ_τ} becomes increasingly larger for $d^i_{QT}(n)$ when τ increases from 20 to 50 s, m_{ϵ_τ} is essentially independent of τ for $\tilde{d}^i_{QT}(n)$ and $\check{d}^i_{QT}(n)$, see Fig. 6. Moreover, using $d^i_{QT}(n)$ for larger values of τ, a large underestimation results during recovery and a large overestimation during exercise which together exaggerate $\Delta\hat{\tau}_p$, defined as the difference between $\hat{\tau}_{p,r}$ and

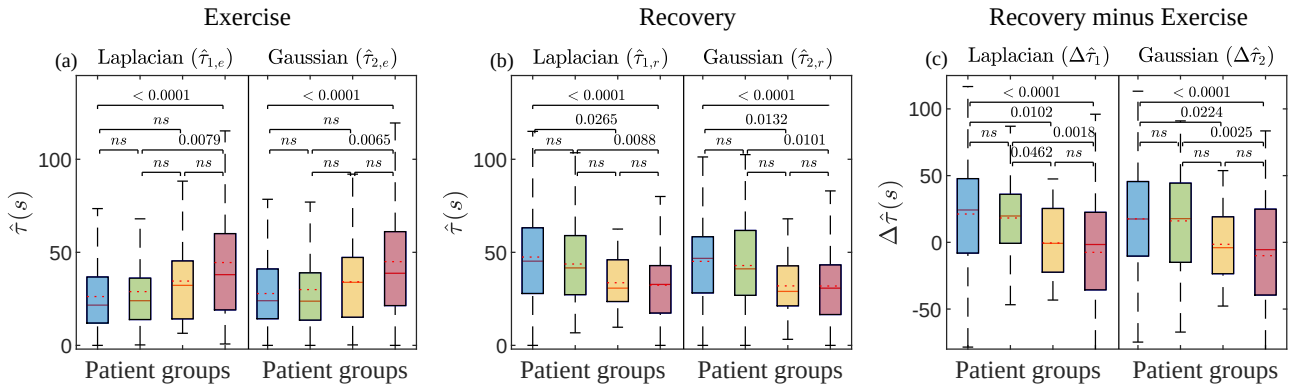

Fig. 9: Box plots of the estimated time delay between $\check{d}^i_{\rm QT}(n)$ and $d_{\rm QT}(n)$ for the four patient groups, assuming either a Laplacian or a Gaussian noise model. The estimates are obtained for (a) exercise, resulting in $\hat{\tau}_{1,e}$ and $\hat{\tau}_{2,e}$, and (b) recovery, resulting in $\hat{\tau}_{1,r}$ and $\hat{\tau}_{2,r}$. (c) Box plots of the difference between recovery and exercise, resulting in $\Delta\hat{\tau}_1$ and $\Delta\hat{\tau}_2$. The dotted and continuous lines in red correspond to the mean and the median, respectively. Patient group color code is: ECG-LR (blue), COR-LR (green), COR-MR (yellow), and COR-HR (red). The delay significance, p-values, in separating patient groups, are plotted above box plot pairs.

$\hat{\tau}_{p,e}$, cf. (5). Consequently, $\Delta\hat{\tau}_p$ is poorly suited to characterize the underlying physiological mechanisms when using $d^i_{\rm QT}(n)$.

In terms of m_{ϵ_τ}, $\check{d}^i_{\rm QT}(n)$ offers better performance than $\tilde{d}^i_{\rm QT}(n)$ since m_{ϵ_τ} is somewhat closer to 0 for most values of τ and SNRs. For example, analysis of the exercise phase of $\mathcal{D}_t$ using $\tau = 50$ s and SNR $= 40$ dB results in $m_{\epsilon_\tau} = 4.3$ s and 2.4 s for $\tilde{d}^i_{\rm QT}(n)$ and $\check{d}^i_{\rm QT}(n)$, respectively, see Fig. 6(d). The results for recovery have about the same magnitude as those for exercise, but with reversed sign, -3.9 s and -2.3 s.

As noted in Sec. V-C, the lower m_{ϵ_τ} for $\tilde{d}^i_{\rm QT}(n)$ and $\check{d}^i_{\rm QT}(n)$ observed during exercise is traded for a higher standard deviation σ_{ϵ_τ}. This is due to the better learning achieved for data pairs in the exercise window, either only in the first half of the window when determining $\Delta_{\rm QT}$ to compute $\tilde{d}^i_{\rm QT}(n)$ or entirely when aligning the window end to peak exercise before $\check{d}^i_{\rm QT}(n)$ is computed. It should be noted that the decrease in m_{ϵ_τ} is larger than the increase in σ_{ϵ_τ}.

B. Estimation of α and β

The data pairs in the exercise window profoundly influence the estimation of α and β and consequently the time lag estimation. This is corroborated by the results obtained from $\mathcal{D}_{ee}$ which show that $[d_{\rm QT}(n), d_{\rm RR}(n)]$ should be selected so that the QT interval achieves its actual stationary value corresponding to the current heart rate, which would produce accurate estimates. Since the data pairs in the exercise window of $\mathcal{D}_t$ and $\mathcal{D}_r$ are nonstationary, data-dependent modification is necessary to obtain better accuracy of $\hat{\alpha}$ and $\hat{\beta}$. In addition, the data pairs from the exercise window of $\mathcal{D}_t$ and $\mathcal{D}_r$ include a wider range of the RR intervals, i.e., from $\tilde{d}^i_{\rm QT}(n)$, or $\check{d}^i_{\rm QT}(n)$, than the pairs selected in a window with stationary data, i.e., from $\mathcal{D}_{ee}$, see Fig. 8. This strategy leads to better fitting of $g(d_{\rm RR}(n); \alpha, \beta)$ in $\mathcal{D}_t$ and $\mathcal{D}_r$ with $\tilde{d}^i_{\rm QT}(n)$, or $\check{d}^i_{\rm QT}(n)$ as compared to that in $\mathcal{D}_{ee}$ with $d^i_{\rm QT}(n)$.

The discrepancy between α, β and $\hat{\alpha}_s$, $\hat{\beta}_s$ is likely a consequence of how the delineator handles T-waves at different heart rates, i.e., different T-wave widths. The wavelet-based delineator makes use of time-invariant filters which modify the width of T-waves, narrower at high heart rates, since higher frequencies can be filtered out. Thus, the behavior of the delineator differs for T-waves at high and low heart rates. Therefore, $\hat{\alpha}_s$ and $\hat{\beta}_s$ represent better reference values than α and β to evaluate performance, since differences in estimates can only be attributed to differential time lag estimation performance in data pair selection for computation of $d^i_{\rm QT}(n)$, $\tilde{d}^i_{\rm QT}(n)$, or $\check{d}^i_{\rm QT}(n)$, see Table III.

C. T-wave end delineation

The results in Table II show that GπCA$_1$ and GπCA$_3$ yield significantly lower delineation errors ϵ_θ than PCA at a low SNR (27 dB), whereas the differences in performance at higher SNRs are negligible. Thus, since the SNR is typically low during exercise, the GπCA-based techniques are better suited for delineation. Accordingly, wave periodicity is a more adequate criterion than variance to determine the best transformed lead for T-wave end delineation.

The present results on delineation agree with those reported in [14], although a known T-wave end reference was lacking in that study. However, the lack was overcome by using the beat-to-beat variability of the observed QT series as a reference, assumed to be composed of natural variability and delineation errors. Moreover, the results agree with those obtained when Holter recordings were analyzed, either obtained from patients in permanent atrial fibrillation [9] or patients suffering from end-stage renal disease [26].

Convolutional neural networks have recently been proposed for QT interval delineation [27]–[29], with performance results similar to those obtained with wavelet analysis [16]. However, the dynamic scenario of EST may prove a challenge to methods based on machine learning.

D. ECG simulation

Out of the many parameters defining the simulator, the time lag and the SNR were deemed to be of primary interest to investigate. When it comes to heart rate, also playing a central role, the results obtained from simulated ECGs with a linearly increasing heart rate trend during exercise are almost identical to those obtained from simulated ECGs with a real heart rate measured during exercise, see Fig. 6; the same observation applies to a linearly decreasing heart rate trend during recovery. These results provide experimental evidence of the theoretical results derived in Appendix II, showing that the assumption of a linearly changing heart rate trend can be broadened to apply to low-frequency changes in the heart rate trend with frequency content below 0.006 Hz.

The noise added to simulated, noise-free ECGs is composed of muscle noise and motion artifacts [15]; baseline wander is not part of the simulator as appropriate correction techniques are available today. While the muscle noise model was specifically designed with reference to EST, the motion artifact model was designed with reference to ambulatory ECGs. Although the simulated motion artifacts resemble those observed during EST, the model can be improved to closer resemble the real-life scenario, e.g., with respect to artifact shape and occurrence probability pattern.

E. Clinical results

The tendency of the estimated time lag follows a pattern similar to the one in [14]: a prolongation during exercise and a shortening during recovery associated with increased CAD risk. A reduced difference between these two time lags is also observed in high-risk CAD patients, see [14] for further discussion. Statistical significance is presented in Fig. 9(c) showing similar results to those presented in [21], obtained from the dataset described in Sec. IV. The most prominent difference is that the discrimination between the COR-LR and the COR-MR groups is statistically significant here when using $\Delta\hat{\tau}_1$, while not so in [21]. This improvement is a consequence of using the robust Laplacian estimator and an improved definition of the learning window at exercise to estimate α and β.

F. Limitations

This work assumes that τ remains constant for each individual. However, studies have shown that QT-RR adaptation depends on the level of sympathetic activation [11], [12], and that the relation between QT and RR varies during exercise and recovery. It is unclear whether the differences in QT adaptation are only due to the varying time lag represented by $h(n)$ or also due to the differing QT-RR memoryless relation. Although the differences between exercise and recovery are accounted for by computing a time lag estimate for each phase, the increasing sympathetic activation during exercise suggests that further research is needed to fully explore this aspect.

VII. Conclusions

Using simulated ECGs, the performance evaluation of the proposed method shows that the estimated QT-RR adaptation time lag agrees well with the true time lag. The original assumption of linear changes in heart rate trends is broadened to also apply to more realistic, low-frequency trends. Moreover, the Laplacian-based estimator better discriminates patients with different risk of suffering from coronary artery disease.

Appendix I
Interchangeability of QT-RR Model Blocks

This appendix shows that the input–output relation of the model in Fig. 1 is approximately equal to the model with reversed block order in Fig. 10, introduced in [5]. In mathematical terms, the modeled QT series of Fig. 1 is given by

$$d_{\mathrm{mQT}}(n) = \sum_{m=0}^{\infty} g(d_{\mathrm{RR}}(n-m))h(m), \tag{11}$$

which thus is approximately equal to the model with reversed order, denoted $d^r_{\mathrm{mQT}}(n)$. For convenience, $g(d_{\mathrm{RR}}(n);\alpha,\beta)$ is shortened to $g(d_{\mathrm{RR}}(n))$.

The starting point is to truncate the sum in (11) to only include the first $M \approx 5\tau$ samples of $h(n)$ as the remaining samples have negligible significance. Thus,

$$d_{\mathrm{mQT}}(n) \approx \sum_{m=0}^{M} g(d_{\mathrm{RR}}(n-m))h(m). \tag{12}$$

Then, since $d_{\mathrm{RR}}(n-m)$ typically exhibits small changes around $d_{\mathrm{RR}}(n)$ in the interval $m \in [0, M]$, the first-order approximation of the Taylor series expansion of $g(d_{\mathrm{RR}}(n-m))$ around $d_{\mathrm{RR}}(n)$ becomes

$$d_{\mathrm{mQT}}(n) \approx \sum_{m=0}^{M} \left[g(d_{\mathrm{RR}}(n)) + g'(d_{\mathrm{RR}}(n))(d_{\mathrm{RR}}(n-m) - d_{\mathrm{RR}}(n))\right] h(m), \tag{13}$$

where $g'(d_{\mathrm{RR}}(n))$ denotes the first derivative. Assuming that $h(n)$ has unitary gain at zero frequency, the first-order approximation becomes

$$d_{\mathrm{mQT}}(n) \approx g(d_{\mathrm{RR}}(n)) + g'(d_{\mathrm{RR}}(n))(d^i_{\mathrm{RR}}(n) - d_{\mathrm{RR}}(n)), \tag{14}$$

where $d^i_{\mathrm{RR}}(n) = \sum_{m=0}^{M} d_{\mathrm{RR}}(n-m)h(m)$. The series $d^i_{\mathrm{RR}}(n)$ can be interpreted as the expected memoryless RR interval series corresponding to the observed $d_{\mathrm{QT}}(n)$ under stationary conditions. By scrutinizing (14), it becomes clear that this expression is a Taylor series approximation of the memoryless transformation which relates $d^i_{\mathrm{RR}}(n)$ to $d_{\mathrm{QT}}(n)$ around $d_{\mathrm{RR}}(n)$,

$$\begin{aligned} d_{\mathrm{mQT}}(n) &\approx g(d^i_{\mathrm{RR}}(n)) = g\left(\sum_{m=0}^{M} d_{\mathrm{RR}}(n-m)h(m)\right) \\ &\approx g\left(\sum_{m=0}^{\infty} d_{\mathrm{RR}}(n-m)h(m)\right) = d^r_{\mathrm{mQT}}(n), \end{aligned} \tag{15}$$

demonstrating the interchangeability of the model blocks in Fig. 1 under the refereed assumptions.

Considering a τ of about 25 s during exercise, the effective length of $h(n)$ is about 5τ corresponding to about 125 s,

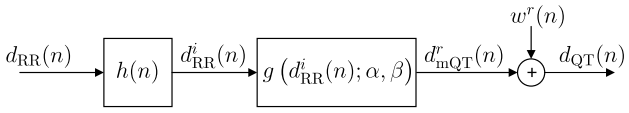

Fig. 10: QT-RR model with a reversed block order, cf. Fig. 1. Note that the reverted estimate of the QT series, $d^r_{\mathrm{mQT}}(n)$, and the reverted modeling plus delineation error, $w^r(n)$, differ from their equivalent in Fig.1 , but the sum results in the observed $d_{\mathrm{QT}}(n)$ series in both cases, $d_{\mathrm{QT}}(n) = d^r_{\mathrm{mQT}}(n) + w^r(n)$.

implying RR changes of as much as 100 ms ($\approx$ 5 bpm) [14]. During recovery, values of τ corresponding to about 50 s should rather be considered, implying RR changes as large as 200 ms ($\approx$ 10 bpm). Several definitions of $g(d_{\mathrm{RR}}(n))$ were considered in [5], all defined so that RR changes as small as 100 ms or 200 ms are well-approximated by a linear QT dependence in the time span of the QT memory, thus supporting the above derivation and the interchangeability of the model blocks in Fig. 1. The basis of the approximation can be observed in Fig. 8 for the hyperbolic transformation, defined in (7).

Appendix II
Conditions on Heart Rate and QT Trend in Time Lag Estimation

The discrete-time Fourier transform of $h(n)$ in (1) is given by

$$H(\omega) = \frac{\kappa}{1 - e^{-1/\tau} e^{-j\omega}}. \tag{16}$$

For healthy subjects, for which τ corresponds to about 25 s [5] and, accordingly, a cut-off frequency F_c of about 0.006 Hz ($\omega \approx 0.01$), the magnitude function of $H(\omega)$ can be approximated for $\omega \ll 0.01$ by

$$|H(\omega)| = \frac{\kappa}{\sqrt{1 - 2e^{-1/\tau}\cos(w) + e^{-2/\tau}}} \approx \frac{\kappa e^{1/\tau}}{e^{1/\tau} - 1}. \tag{17}$$

For $1/\tau \ll 1$, the phase function $\angle H(\omega)$ can be approximated by

$$\angle H(\omega) = -\arctan\left(\frac{\sin(w)}{e^{1/\tau} - \cos(w)}\right) \approx -\frac{\omega}{e^{1/\tau} - 1} \approx -\omega\tau, \tag{18}$$

resulting in the following approximate expression of $H(\omega)$:

$$H(\omega) \approx \frac{\kappa e^{1/\tau}}{e^{1/\tau} - 1} e^{-j\omega\tau}, \tag{19}$$

which is a pure delay for frequencies below F_c. The constant κ is chosen so that the gain is unitary.

Consequently, in order to estimate τ by measuring the delay between $d_{\mathrm{QT}}(n)$ and $d^i_{\mathrm{QT}}(n)$, the QT trend $s(n)$ does not need to be a linear ramp, but it is enough if its frequency content is below F_c. It should be noted that most of the frequency content in real heart rate trends is below the very low-frequency band of heart rate variability, defined by [0.0033, 0.04] Hz [30].

References

[1] P. Laguna, J. P. Martínez, and E. Pueyo, "Techniques for ventricular repolarization instability assessment from the ECG," *Proc. IEEE*, vol. 104, no. 2, pp. 392–415, 2016.

[2] H. Gravel, V. Jacquemet, N. Dahdah, and D. Curnier, "Clinical applications of QT/RR hysteresis assessment: a systematic review," *Ann. Noninvasive Electrocardiol.*, vol. 23, no. 1, p. e12514, 2018.

[3] J. T. Tikkanen, T. Kentta, K. Porthan, O. Anttonen, A. Eranti, A. L. Aro, T. Kerola, H. A. Rissanen, P. Knekt, M. Heliövaara *et al.*, "Risk of sudden cardiac death associated with QRS, QTc, and JTc intervals in the general population," *Heart Rhythm*, vol. 19, no. 8, pp. 1297–1303, 2022.

[4] J. Ramírez, M. Orini, A. Mincholé, V. Monasterio, I. Cygankiewicz, A. Bayes de Luna, J. P. Martínez, E. Pueyo, and P. Laguna, "T-wave morphology restitution predicts sudden cardiac death in patients with chronic heart failure," *J. Am. Heart Ass.*, vol. 6, no. 5, p. e005310, 2017.

[5] E. Pueyo, P. Smetana, P. Caminal, A. Bayes de Luna, M. Malik, and P. Laguna, "Characterization of QT interval adaptation to RR interval changes and its use as a risk-stratifier of arrhythmic mortality in amiodarone-treated survivors of acute myocardial infarction," *IEEE Trans. Biomed. Eng.*, vol. 51, no. 9, 2004.

[6] P. Kligfield, K. G. Lax, and P. M. Okin, "QT interval-heart rate relation during exercise in normal men and women: definition by linear regression analysis," *J. Am. Coll. Cardiol.*, vol. 28, no. 6, 1996.

[7] P. Smetana, E. Pueyo, K. Hnatkova, V. Batchvarov, P. Laguna, and M. Malik, "Individual patterns of dynamic QT/RR relationship in survivors of acute myocardial infarction and their relationship to antiarrhythmic efficacy of amiodarone," *J. Cardiovasc. Electrophysiol.*, vol. 15, no. 10, pp. 1147–1154, 2004.

[8] A. Grom, T. S. Faber, M. Brunner, C. Bode, and M. Zehender, "Delayed adaptation of ventricular repolarization after sudden changes in heart rate due to conversion of atrial fibrillation. A potential risk factor for proarrhythmia?" *EP Europace*, vol. 7, no. 2, pp. 113–121, 2005.

[9] A. Martín-Yebra, L. Sörnmo, and P. Laguna, "QT interval adaptation to heart rate changes in atrial fibrillation as a predictor of sudden cardiac death," *IEEE Trans. Biomed. Eng.*, vol. 69, no. 10, pp. 3109–3118, 2022.

[10] E. Pueyo, Z. Husti, T. Hornyik, I. Baczkó, P. Laguna, A. Varró, and B. Rodríguez, "Mechanisms of ventricular rate adaptation as a predictor of arrhythmic risk," *Am. J. Physiol. Heart Circ. Physiol.*, vol. 298, no. 5, pp. H1577–H1587, 2010.

[11] D. A. Sampedro-Puente, J. Fernandez-Bes, N. Szentandrássy, P. P. Nánasi, and E. Pueyo, "Time course of low-frequency oscillatory behavior in human ventricular repolarization following enhanced sympathetic activity and relation to arrhythmogenesis," *Front. Physiol.*, vol. 10, p. 1547, 2020.

[12] C. Pérez, R. Cebollada, K. A. Mountris, J. P. Martínez, P. Laguna, and E. Pueyo, "The role of β-adrenergic stimulation in QT interval adaptation to heart rate during stress test," *Plos One*, vol. 18, no. 1, p. e0280901, 2023.

[13] J. Barker, X. Li, S. Khavandi, D. Koeckerling, A. Mavilakandy, C. Pepper, V. Bountziouka, L. Chen, A. Kotb, I. Antoun *et al.*, "Machine learning in sudden cardiac death risk prediction: a systematic review," *Europace.*, vol. 24, pp. 1777–1787, 2022.

[14] C. Pérez, E. Pueyo, J. P. Martínez, J. Viik, and P. Laguna, "QT interval time lag in response to heart rate changes during stress test for coronary artery disease diagnosis," *Biomed. Signal Process. Control*, vol. 86, p. 105056, 2023.

[15] L. Bachi, H. Halvaei, C. Pérez, A. Martín-Yebra, A. Petrénas, A. Solosenko, L. Johnson, V. Marozas, J. P. Martínez, E. Pueyo, M. Stridh, P. Laguna, and L. Sörnmo, "ECG modeling for simulation of arrhythmias in time-varying conditions," *IEEE Trans. Biomed. Eng.*, vol. 70, no. 12, pp. 3449–3460, 2023.

[16] J. P. Martínez, R. Almeida, S. Olmos, and P. Laguna, "A wavelet-based ECG delineator: evaluation on standard databases," *IEEE Trans. Biomed. Eng.*, vol. 51, no. 4, 2004.

[17] F. Castells, P. Laguna, L. Sörnmo, A. Bollmann, and J. M. Roig, "Principal component analysis in ECG signal processing," *J. Adv. Signal Process.*, vol. 2007, pp. 1–21, 2007.

[18] C. Meyer and H. Keiser, "Electrocardiogram baseline noise estimation and removal using cubic splines and state-space computation techniques," *Comput. Biomed. Res.*, vol. 10, no. 5, pp. 459–470, 1977.

[19] E. Pueyo, M. Malik, and P. Laguna, "A dynamic model to characterize beat-to-beat adaptation of repolarization to heart rate changes," *Biomed. Signal Process. Control*, vol. 3, no. 1, pp. 29–43, 2008.

[20] K. Ogata, *Modern Control Engineering, Instrumentation and Controls*. Prentice Hall, 2010.

[21] S. Romagnoli, C. Peréz, L. Burattini, E. Pueyo, M. Morettini, A. Sbrollini, J. P. Martínez, and P. Laguna, "Model-based estimators of QT series time delay in following Heart-Rate changes," *45th Ann. Int. Conf. IEEE Eng. Med. Biol. Soc. (EMBC)*, pp. 1–4, 2023.

[22] R. Bailón, J. Mateo, S. Olmos, P. Serrano, J. García, A. Del Río, I. Ferreira, and P. Laguna, "Coronary artery disease diagnosis based on exercise electrocardiogram indexes from repolarisation, depolarisation and heart rate variability," *Med. Biol. Eng. Comput.*, vol. 41, no. 5, pp. 561–571, 2003.

[23] A. Petrenas, V. Marozas, A. Sološenko, R. Kubilius, J. Skibarkiene, J. Oster, and L. Sörnmo, "Electrocardiogram modeling during paroxysmal atrial fibrillation: application to the detection of brief episodes," *Physiol. Meas.*, vol. 38, no. 11, p. 2058, 2017.

[24] R. Bailón, L. Sornmo, and P. Laguna, "A robust method for ECG-based estimation of the respiratory frequency during stress testing," *IEEE Trans. Biomed. Eng.*, vol. 53, no. 7, pp. 1273–1285, 2006.

[25] M. Virtanen, M. Kähönen, T. Nieminen, P. Karjalainen, M. Tarvainen, T. Lehtimäki, R. Lehtinen, K. Nikus, T. Kööbi, M. Niemi *et al.*, "Heart rate variability derived from exercise ECG in the detection of coronary artery disease," *Physiol. Meas.*, vol. 28, no. 10, p. 1189, 2007.

[26] F. Palmieri, P. Gomis, J. E. Ruiz, D. Ferreira, A. Martín-Yebra, E. Pueyo, J. P. Martínez, J. Ramírez, and P. Laguna, "ECG-based monitoring of blood potassium concentration: Periodic versus principal componentas lead transformation for biomarker robustness," *Biomed. Signal Process. Control*, vol. 68, no. 102719, 2021.

[27] G. Jimenez-Perez, A. Alcaine, and O. Camara, "Delineation of the electrocardiogram with a mixed-quality-annotations dataset using convolutional neural networks," *Scientific reports*, vol. 11, 12 2021.

[28] M. S. Haleem and L. Pecchia, "A deep learning based ecg segmentation tool for detection of ecg beat parameters," *Proceedings - IEEE Symposium on Computers and Communications*, vol. 2022-June, 2022.

[29] M. D. Diaw, S. Papelier, A. Durand-Salmon, J. Felblinger, and J. Oster, "AI-assisted QT measurements for highly automated drug safety studies," *IEEE Trans. Biomed. Eng.*, vol. 70, pp. 1504–1515, 5 2023.

[30] Task Force of the European Society of Cardiology and the North American Society of Pacing Electrophysiology, "Heart rate variability: standards of measurement, physiological interpretation and clinical use," *Circulation*, vol. 93S, pp. 1043–1065, 1996.